remote sensing

MDPI

Article

Dynamic Water Quality Changes in the Main Stream of the Yangtze River from Multi-Source Remote Sensing Data

Jiarui Zhao [1,2], Shuanggen Jin [2,3,4,*] and Yuanyuan Zhang [3]

[1] School of Communication and Information Engineering, Shanghai University, Shanghai 200444, China
[2] Shanghai Astronomical Observatory, Chinese Academy of Sciences, Shanghai 200030, China
[3] School of Remote Sensing and Geomatics Engineering, Nanjing University of Information Science and Technology, Nanjing 210044, China
[4] School of Surveying and Land Information Engineering, Henan Polytechnic University, Jiaozuo 454000, China
* Correspondence: sgjin@shao.ac.cn or sgjin@nuist.edu.cn

Abstract: Total nitrogen (TN) and total phosphorus (TP) are important indicators of water quality. Although water quality can be obtained with high accuracy using traditional measurement methods, the cost is high and the area is limited. In the past a single-satellite remote sensing system was normally used to estimate water quality at a large scale, while bands were fewer with limited accuracy. In this paper, inversion models for TN and TP are obtained and validated in the main stream of the Yangtze River using multi-source remote sensing data. The joint inversion models for TN and TP have higher accuracy ($R^2 = 0.81$ *and* 0.86, $RMSE = 0.51$ *and* 0.10 mg L^{-1}) than the single-satellite inversion models ($R^2 = 0.61 - 0.62$ *and* $0.59 - 0.75$, $RMSE = 0.41 - 0.61$ *and* $0.07 - 0.12$ mg L^{-1}). Using these models, water quality changes in the Yangtze River are obtained from 2019 to 2021. It is found that TN and TP in the upstream and downstream are high. In spring and autumn, the water quality is poor. The water quality in the Yangtze River is mostly Class III with improvement. Furthermore, it is found that TN and TP are negatively correlated with the water level, temperature and flow in Jiujiang. The p value between water quality and the water level is higher than for other factors, with -0.76 and -0.64 for TN and TP, respectively.

Keywords: total nitrogen; total phosphorus; Landsat-8; Sentinel-2A; Yangtze River

Citation: Zhao, J.; Jin, S.; Zhang, Y. Dynamic Water Quality Changes in the Main Stream of the Yangtze River from Multi-Source Remote Sensing Data. *Remote Sens.* **2023**, *15*, 2526. https://doi.org/10.3390/rs15102526

Academic Editor: SeungHyun Son

Received: 28 February 2023
Revised: 11 April 2023
Accepted: 2 May 2023
Published: 11 May 2023

1. Introduction

The Yangtze River is the largest river in China, which spans as many as 11 provinces, municipalities and autonomous regions in China. In recent years, China has planned an economic belt along the Yangtze River with an area of more than 2 million square kilometers. The economy of the main stream of the Yangtze River has developed rapidly [1]. However, with the rapid development of the economy, the water quality and surrounding environment of the main stream of the Yangtze River are also suffering from more and more serious pollution. According to the research of biological and ecological environment experts and the data reported by the national government, the water of the main stream of the Yangtze River has been seriously damaged [2,3]. The large amount of household waste generated by residents of the Yangtze River Basin not only leads to an increase in local carbon emissions, but also increases the content of salt-containing organic matter in the water due to the presence of waste incineration plants [4,5]. A large number of breeding and chemical enterprises that rely on the resources of the main stream of the Yangtze River also discharge a large amount of breeding feed containing nitrogen and phosphorus and industrial wastewater containing heavy metal ions into the river. Moreover, the water quality of the main stream of the Yangtze River has deteriorated and even affected the water quality of other lakes and tributaries in the Yangtze River Basin, resulting in the eutrophication of the water. Hui and Yao established a TP inversion model of Poyang Lake using MODIS data, and the results showed that the average eutrophication degree of the

lake was 59.8% [6]. Lu et al. found that different landscape structures have a significant impact on the content of heavy metals in Xiangjiang [7]. Shang et al.'s results show that TP in Taihu Lake has increased by 17.3% in the past seven years [8]. Monitoring and remote sensing data continue to show that planning and water management strategies for the water quality and water environments of the main stream of the Yangtze River need to be developed and implemented [9,10].

The traditional water quality monitoring method calls for water samples to be collected and analyzed for chemicals and evaluated according to certain standards [11]. Data obtained through this method typically have high accuracy and reliable results for the water quality of sampling points at a specific time. However, this method is time-consuming and laborious with high costs. It is difficult to comprehensively analyze the water quality and changing trends in water bodies across time and space through several sampling points in a specific time.

With the development of remote sensing technology, satellite remote sensing data can be used to estimate water quality. The estimated parameters include total nitrogen (TN), total phosphorus (TP), dissolved oxygen and so on [12,13]. When using remote sensing data for water quality inversion, the content of water quality parameters in the water body has to be obtained through sampling and chemical analysis. Then, based on the content of water quality parameters and the band reflectance data of remote sensing image data, a water quality inversion model with high correlation can be constructed. A network can also be used to realize high-precision water quality inversion [14–16]. Finally, the verification and accuracy analysis of the model are carried out to obtain a more reliable inversion model. Compared with the traditional method, the cost of this method is greatly reduced, and a wider range of water quality monitoring can be realized. The obtained water quality inversion model can realize continuous monitoring across time and space, and it is conducive to reflecting and analyzing the water quality and changing trends in water bodies through images. If necessary, the results can be obtained quickly. When the water quality changes significantly, the model can be modified via adding measured data to obtain a sustainable water quality inversion model.

TN and TP are important indicators for evaluating water quality, which can be used for both qualitative and quantitative research [17]. In this research, these two water quality parameters are obtained and studied for water quality. At present, there are many results for water quality inversion using remote sensing data, and the technologies and methods are relatively mature. Isenstein and Park used the method of multiple linear regression and Landsat-enhanced thematic mapper plus (ETM +) imagery to establish TN and TP inversion models (R^2 = 0.81 and 0.75) [18]. A water eutrophication distribution map of Lake Champlain and Missisquoi Bay was calculated, which proved extension for other eutrophic lakes. Singh and Jha collected water samples on the date of passage of a Landsat-8 satellite through the Ganga River and used Landsat-8 image data to build a nonlinear equation to calculate the total suspended solids (TSS) in the water [19]. He et al. used Landsat-8 remote sensing satellite data and the polynomial fitting method, and TN and TP in the main stream of the Yangtze River were estimated from 2014 to 2020. The correlation of TN and TP was more than 0.8, though there was a lack of an accuracy test for the models [20]. Du et al. used GOCI remote sensing images to estimate the inverse TP of Taihu Lake through regression analysis and the highest accuracy of the model was obtained with correction 0.898 [21].

Recent research has mainly focused on small and non-flowing lakes or rivers, while there is a lack of study in large and flowing rivers, such as the Yangtze River. In addition, only single-satellite data was used. The number and wavelength of different remote sensing satellites are different, and the sensitivity to TN and TP is also different. Masoud believed that multi-source satellite joint inversion will obtain a more accurate water quality inversion model [22]. Furthermore, the impact of natural factors on water quality is still not clear, such as the space-time scale. Numerous researches have shown that changes in the natural environment and the land types around the water body or human daily life will affect local

water quality [23,24]. The magnitude of the impact caused by these factors, or their positive and negative significance, should be further explored.

In this study, the remote sensing data of Landsat-8 and Sentinel-2A and measured data are used to carry out single-satellite inversion and joint inversion based on multi-source remote sensing data for TN and TP in the main stream of the Yangtze River. The accuracy of the inversion model is validated. Through the obtained water quality inversion model, the changing trend of TN and TP in the Yangtze River over the past three years is obtained. Finally, the causes of changes in water quality are further discussed based on other hydrological and meteorological data.

2. Materials and Methods

2.1. Study Area

The Yangtze River, with a total length of about 6300 km, originates from Tanggula Mountain in Qinghai Province and flows into the East China Sea near Chongming Island in Shanghai. The whole Yangtze River Basin covers an area of about 1.8 million square kilometers, spanning Eastern, Central and Western China. In this research, the main stream of the Yangtze River, located at 24–36 degrees north latitude and 105–120 degrees east longitude, was selected as the study area. The basin is rich in water conservancy resources, biological resources and mineral resources. At the same time, it is also a hub of transportation and an important engine of China's economic development. Good water quality is an important guarantee for the normal operation of these industries, so it is necessary to conduct long-term and comprehensive monitoring and analysis of the water quality in the main stream of the Yangtze River.

2.2. Data

2.2.1. Remote Sensing Data

Here Landsat-8 and Sentinel-2A images were downloaded from Google Earth Engine. The data sets were the Landsat-8 OLI/TIRS Surface Reflectance dataset (LANDSAT/LC08/C01/T1_SR) and Sentinel-2A Surface Reflectance dataset (COPERNICUS/S2_SR), from June to October 2021. Landsat-8 images contain 7 bands (b_1, b_2, ... b_7), with a wavelength range of 0.435–2.294 microns and a resolution of 30 m, as shown in Table 1. Sentinel-2A images contain 12 bands (b_1, b_2, ..., b_{12}), with a wavelength range of 0.4439–2.2024 microns and a resolution of 10–60 m, as shown in Table 2.

Table 1. List of Landsat-8's bands.

Band	Wavelength (μm)	Size (m)
b_1 (Ultra blue)	0.435–0.451	30
b_2 (Blue)	0.452–0.512	30
b_3 (Green)	0.533–0.590	30
b_4 (Red)	0.636–0.673	30
b_5 (Near infrared)	0.851–0.879	30
b_6 (Shortwave infrared1)	1.566–1.651	30
b_7 (Shortwave infrared2)	2.107–2.294	30

Table 2. List of Sentinel-2A's bands.

Band	Wavelength (μm)	Size (m)
b_1 (Aerosols)	0.4439	60
b_2 (Blue)	0.4966	10
b_3 (Green)	0.5600	10
b_4 (Red)	0.6645	10
b_5 (Red edge1)	0.7039	20
b_6 (Red edge2)	0.7402	20
b_7 (Red edge3)	0.7825	20
b_8 (Near infrared)	0.8351	10
b_{8A} (Red edge4)	0.8648	20
b_{10} (Water vapor)	0.9450	60
b_{11} (SWIR1)	1.6137	20
b_{12} (SWIR2)	2.2024	20

2.2.2. In-Situ Measurements

The data sources of measured TN and TP used in this research have two parts. In the first part, the research team of Shanghai Astronomical Observatory, Chinese Academy of Sciences (SHAO) and Nanjing University of Information Science and Technology (NUIST) measured a total of 200 points in Nanjing, Jiujiang, Yueyang and Yichang in September 2021 and 50 additional points in Nanjing in October, and the WTW photoLab 7100VIS water quality analyzer was used for water quality analysis. The second part was the water quality measurement of 99 points measured by the Xi'an Institute of Optics and Precision Mechanics, Chinese Academy of Sciences (Xi'an OPT) along the upper and middle reaches of the Yangtze River in June 2021. The measured points are uniformly distributed along the main stream of the Yangtze River, as shown in Figure 1. Firstly, the water in test tubes was collected and stored with reaching as close to the center of river as possible by boat. After returning to the laboratory the water sample stands for about 40 min, and reagents are heated and added according to the experimental requirements. Finally, the processed water sample is placed into the WTW water quality analyzer and the set program is used to measure TN and TP. The effective range is 0–3.5 mg L^{-1} for TN and 0–0.5000 mg L^{-1} for TP. Each sampling operation complies with the technical specifications for water quality sampling issued by the Ministry of Water Resources of the People's Republic of China.

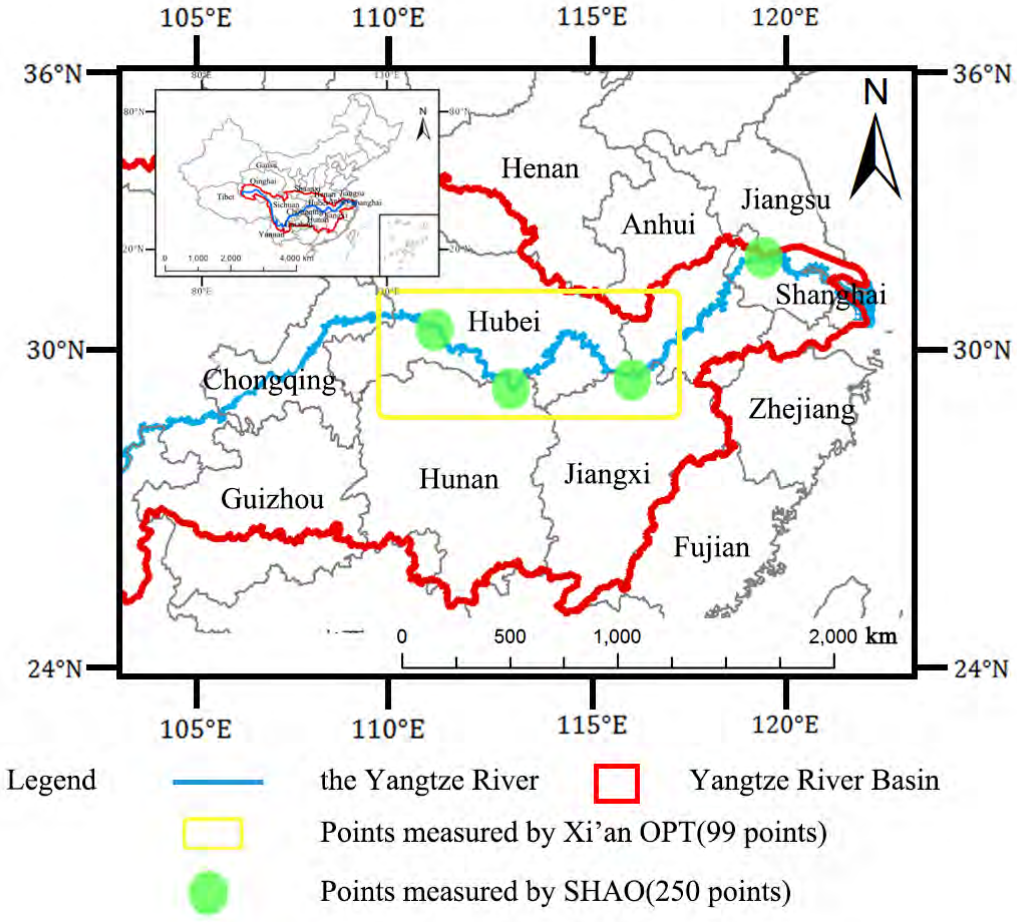

Figure 1. Study area and location of the in-situ measurement sampling points.

2.2.3. Other Data

Other hydrological, meteorological and human factor data were used to analyze the causes of water quality changes. In terms of natural data, the monthly water level, temperature and flow data of Jiujiang hydrological monitoring station from 2019 to 2021 were selected. The water level and flow data are publicly available on the official website of the Changjiang Maritime Safety Administration (cj.msa.gov.cn, accessed on 1 June 2022).

The frequency of water level data updates is twice a day, and the frequency of flow data updates is once a day. The temperature data was sourced from Weather China (www.weather.com.cn, accessed on 1 June 2022), with a frequency of once a day. In this study, monthly mean values were calculated and applied to water level, temperature and flow data. Data such as urbanization change rate and enterprise land change in the area of Jiujiang from 2019 to 2021 were published by the Jiujiang Municipal People's Government (available at https://www.jiujiang.gov.cn/xxgk/xzwgk/jggk/gzbg/jjzfgzbg, accessed on 1 June 2022).

2.3. Methods

2.3.1. Establishment of Models

Because the accuracy of models obtained via fitting the reflectivity of a single band with measured data is low, the reflectivity of multiple bands was combined first and then used for model construction to improve the accuracy of the inversion model. Twelve empirical feature types have been widely used to study the water quality of inland water bodies and coastal areas in recent years [25,26]. In this research, these feature types will be represented by $F_1, F_2, \ldots, F_{12}$.

F_1 is the frequency band ratio, which is the most common spectral derivative feature. Previous studies have shown that it can be used to estimate the content of chlorophyll-a and TSS [27,28]. F_2 is a standardized difference index such as the water and vegetation index, which has also proved to be applicable for calculating the content of chlorophyll-a in water [29,30]. F_3 has also been proven a strong correlation with chlorophyll-a [31]. F_1–F_3 are defined as follows:

$$F_1 = \frac{b_i}{b_j}, i = \{1, \ldots, N-1\}, j = \{i+1, \ldots, N\} \quad (1)$$

$$F_2 = \frac{b_i - b_j}{\lambda_i - \lambda_j}, i = \{1, \ldots, N-1\}, j = \{i+1, \ldots, N\} \quad (2)$$

$$F_3 = \frac{b_i - b_j}{b_i + b_j}, i = \{1, \ldots, N-1\}, j = \{i+1, \ldots, N\} \quad (3)$$

where b_i and b_j are spectral bands and λ_i and λ_j are the central wavelengths of b_i and b_j.

Another kind of band combination was summarized based on describing the color change of the water body. It is very suitable for developing image processing technology based on human visual description. Recent studies have shown some potential and can be applied and developed [32,33]. F_4–F_6 are defined as follows:

$$F_4 = \begin{cases} \omega \quad if\ b_i \le b_j \\ 360 - \omega \quad if\ b_i \ge b_j \end{cases}, \omega = \cos^{-1}\left\{ \frac{0.5\left[(b_k - b_i) + (b_k - b_j)\right]}{\left[(b_k - b_j)^2 + (b_k - b_j)(b_j - b_i)\right]^2} \right\} \quad (4)$$
$$i = \{1, \ldots, N-2\}, j = \{i+1, \ldots, N-1\}, k = \{j+1, \ldots, N\}$$

$$F_5 = 1 - \frac{3}{b_i + b_j + b_k}\left[\min(b_i, b_j, b_k)\right], i = \{1, \ldots, N-2\} \quad (5)$$
$$j = \{i+1, \ldots, N-1\},\ k = \{j+1, \ldots, N\}$$

$$F_6 = \frac{b_i + b_j + b_k}{3}, i = \{1, \ldots, N-2\}, j = \{i+1, \ldots, N-1\}, k = \{j+1, \ldots, N\} \quad (6)$$

where b_i, b_j and b_k are spectral bands.

Transformation based on spatial coordinate systems has also proved to be effective, including the transformation from a Cartesian coordinate system to a polar coordinate system. The method below transforms a Cartesian coordinate system into a spherical coordinate system and was used to obtain and estimate the information of water quality [26]. F_7–F_9 are defined as follows:

$$F_7 = \tan^{-1}\left(\frac{b_i}{b_j}\right), i = \{1, \ldots, N-1\}, j = \{i+1, \ldots, N\} \quad (7)$$

$$F_8 = \tan^{-1}\left(\frac{b_k}{\sqrt{{b_i}^2+{b_j}^2}}\right), i = \{1, \ldots, N-2\} \quad j = \{i+1, \ldots, N-1\}, k = \{j+1, \ldots, N\} \quad (8)$$

$$F_9 = \sqrt{{b_i}^2 + {b_j}^2 + {b_k}^2},\ i = \{1, \ldots, N-2\},\ j = \{i+1, \ldots, N-1\},\ k = \{j+1, \ldots, N\} \quad (9)$$

where b_i, b_j and b_k are spectral bands.

The direction cosine determines the direction of a vector in space, which also has potential in the study of remote sensing inversion of water quality [34]. In this study, the directional cosine of the spectral band in three-dimensional space is constructed to explore its correlation with the content of water quality parameters. F_{10}–F_{12} are defined as follows:

$$F_{10} = \frac{b_i}{\sqrt{{b_i}^2 + {b_j}^2 + {b_k}^2}}, i = \{1, \ldots, N-2\}, j = \{i+1, \ldots, N-1\}, k = \{j+1, \ldots, N\} \quad (10)$$

$$F_{11} = \frac{b_j}{\sqrt{{b_i}^2 + {b_j}^2 + {b_k}^2}}, i = \{1, \ldots, N-2\}, j = \{i+1, \ldots, N-1\}, k = \{j+1, \ldots, N\} \quad (11)$$

$$F_{12} = \frac{b_k}{\sqrt{{b_i}^2 + {b_j}^2 + {b_k}^2}}, i = \{1, \ldots, N-2\}, j = \{i+1, \ldots, N-1\}, k = \{j+1, \ldots, N\} \quad (12)$$

where b_i, b_j and b_k are spectral bands.

All bands of the remote sensing satellite were combined according to the above 12 empirical band combinations, and the correlation was analyzed in combination with the measured data for TN and TP. Finally, the band combination with the highest correlation with water quality parameters was selected for the study.

2.3.2. Model Accuracy Verification

The selected band combination was fitted to the measured data using polynomial regression, and the correlation (R^2) and root mean square error (RMSE) were used as evaluation criteria to select the polynomial degree most suitable for inversion. A higher correlation and a smaller RMSE suggest better model performance. Then, the measured data used for model verification were substituted into the obtained model for verification, and the RMSE was calculated to evaluate the verification effect.

Through the above work, the inversion models of TN and TP from Landsat-8 and Sentinel-2A's surface reflectance were obtained. To obtain more accurate models, the resolution of Sentinel-2A image data was first resampled to 30 m in Google Earth Engine, matching the resolution of the Landsat-8 image data, because of limited internal storage. Then, the inversion models from different satellites were combined according to different averaging methods, including arithmetic average, geometric average and weighted average based on the correlation of the two models. Finally, the validation group data was substituted into the obtained joint inversion models for validation, and the RMSE was calculated to evaluate the validation effect.

3. Results and Analysis

3.1. Single-Satellite Inversion

3.1.1. Establishment of Models from a Single Satellite

All the measured data were screened according to the effective range of TN (0–3.5 mg L^{-1}) and TP (0–0.5 mg L^{-1}). After the screening, the remaining data were randomly divided into an inversion group and a verification group with the proportion

of about 10:1. The inversion group data and remote sensing satellite data obtained from Google Earth Engine were used for inversion.

Seven bands and twelve bands of Landsat-8 and Sentinel-2A surface reflectance, respectively, were substituted into twelve empirical band combinations for fitting, and the correlation and RMSE of TN and TP were calculated. First, the optimal combination mode was compared in each empirical band combination, and then all empirical band combinations were compared together to obtain the most suitable band combination for inversion. Because different water quality parameters have different sensitivities to different bands, there must be a certain wave band combination whose correlation with TN or TP is the highest. The obtained inversion models, corresponding remote sensing satellites, water quality parameters and evaluation indicators are shown in Figures 2 and 3 and Table 3.

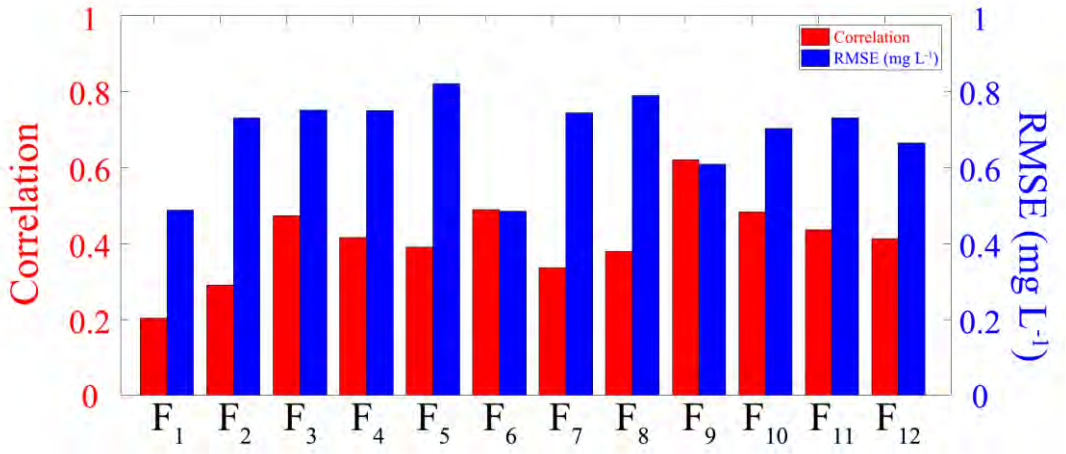

(**a**) Landsat−8 and TN

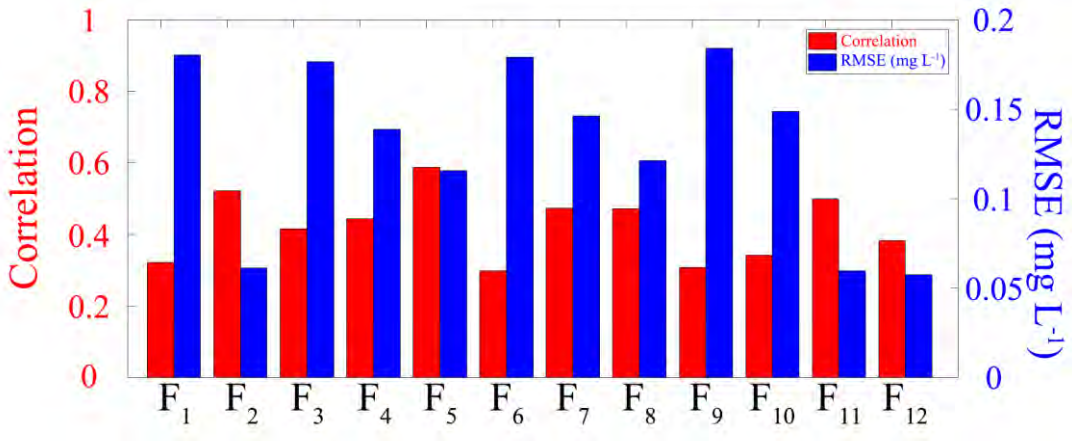

(**b**) Landsat−8 and TP

Figure 2. (**a**) The correlation and RMSE of each band combination of Landsat-8 for TN. (**b**) The correlation and RMSE of each band combination of Landsat-8 for TP.

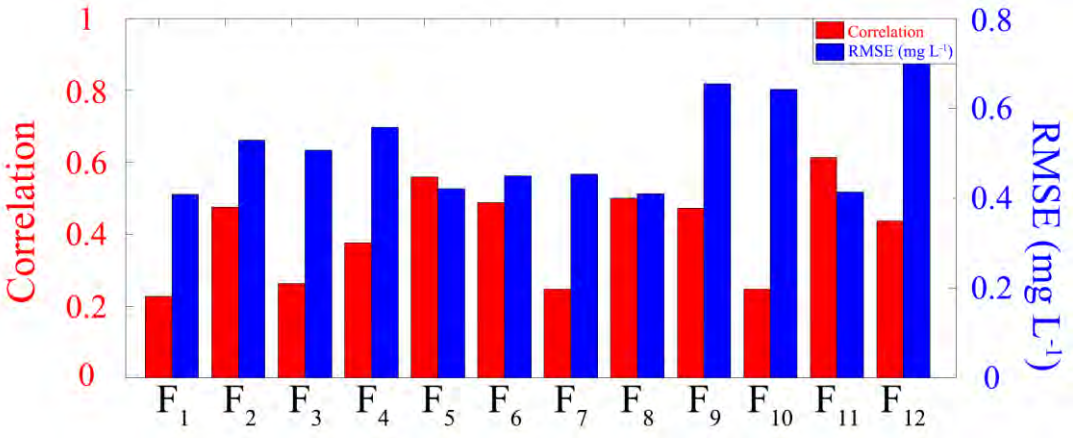

(**a**) Sentinel−2A and TN

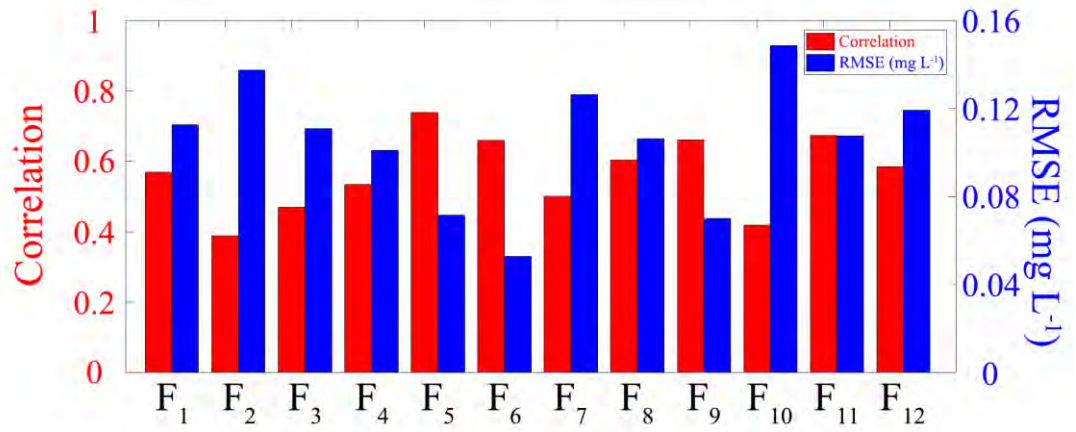

(**b**) Sentinel−2A and TP

Figure 3. (**a**) The correlation and RMSE of each band combination of Sentinel-2A for TN. (**b**) The correlation and RMSE of each band combination of Sentinel-2A about TP.

Table 3. Single-satellite inversion models and evaluation indexes.

Satellites	Water Quality Parameters	Characteristics	Inversion Models	R^2	RMSE (mg L^{-1})
Landsat-8	TN	$F_9 = \sqrt{b_2{}^2 + b_3{}^2 + b_7{}^2}$	$y = 667.9X^3 - 291X^2 + 21.23X + 3.184$	0.62	0.61
	TP	$F_5 = 1 - \frac{3}{b_2+b_3+b_6}[\min(b_2, b_3, b_6)]$	$y = 21.46X^3 - 26.12X^2 + 8.609X - 0.4663$	0.59	0.12
Sentinel-2A	TN	$F_{11} = \frac{b_{11}}{\sqrt{b_8{}^2+b_{11}{}^2+b_{12}{}^2}}$	$y = 581.1X^3 - 979.3X^2 + 536.4X - 93.31$	0.61	0.41
	TP	$F_5 = 1 - \frac{3}{b_7+b_{8A}+b_{11}}[\min(b_7, b_{8A}, b_{11})]$	$y = -33.64X^3 + 19.39X^2 - 1.792X + 0.08766$	0.74	0.07

When the model is constructed, the cubic polynomial was selected for fitting with considering the factors of model accuracy and computational speed. If the polynomial degree is too low, the correlation will be too low to meet the needs. If the polynomial degree is too

high, it will lead to over-fitting. Namely, the polynomial degree and correlation increase, but RMSE increases. The results show that for Landsat-8 data, the band combination of the selected model for retrieving TN is F_9, the correlation is 0.62 and RMSE is 0.61 mg L^{-1}. The band combination of the selected model for the inversion of TP is F_5, the correlation is 0.59 and RMSE is 0.12 mg L^{-1}. In general, the inversion model is more reliable and can be used for further research.

For Sentinel-2A data, the band combination of the selected model for retrieving TN is F_{11}, the correlation is 0.61 and RMSE is 0.41 mg L^{-1}. The band combination of the selected model for inversion of TP is F_5, the correlation is 0.74 and RMSE is 0.07 mg L^{-1}. In general, the inversion model is more reliable and can be used for further research.

3.1.2. Accuracy Analysis

The validation group data were substituted into the inversion models for validation, and RMSE was used as the evaluation index for evaluation. The results are as follows: the RMSE of the validation group of the TN inversion model from Landsat-8 is 0.7204 mg L^{-1}, and the RMSE of the validation group of TP inversion model is 0.1109 mg L^{-1}. The RMSE of the validation group of the TN content inversion model from Sentinel-2A is 0.4834 mg L^{-1}, and the RMSE of the validation group of the constructed TP inversion model is 0.1169 mg L^{-1}. All results are shown in Table 4.

Table 4. Accuracy analysis of single-satellite inversion models.

Inversion Models	Validation Group's RMSE (mg L^{-1})
Landsat-8 about TN	0.72
Landsat-8 about TP	0.11
Sentinel-2A about TN	0.48
Sentinel-2A about TP	0.12

In general, Landsat-8 and Sentinel-2A image data were used to estimate the contents of TN and TP, respectively, which can meet general accuracy requirements, but there is still improvement for correlation and RMSE. In addition, there are abnormal data in the process of comparing the inversion results with the validation group data, which has a great impact on the accurate evaluation of the overall model. In the following section, it is necessary to increase the anti-interference ability of models to make the fitting curve smoother.

3.2. Multi-Source Satellite Inversion

3.2.1. Establishment of Models from Multi-Source Satellites

Through the work in Section 3.1, the models of TN and TP from Landsat-8 and Sentinel-2A data have been obtained. The models have good correlation and low RMSE. In order to further improve the accuracy of the inversion models and the ability of the models, further study is needed for the inversion models of TN and TP from joint multi-source satellites.

For the TN model from Landsat-8 and Sentinel-2A, there are six methods for being combined: square average, arithmetic average, geometric average, harmonic average, weighted average according to correlation and weighted average according to RMSE. In this study, the correlation and RMSE calculated through various joint methods were compared, and finally the optimal joint method was selected. The water quality parameters and evaluation indexes of the joint inversion model are shown in Figure 4 and Table 3.

For TN, the RMSEs of the models obtained via several joint inversion methods were similar, so the square average method with the highest correlation was selected to build the inversion model. The correlation is 0.81 and the RMSE is 0.51 mg L^{-1}. For TP, although the RMSE of the model obtained using the harmonic average method was large, its correlation was much higher than other methods. The correlation is 0.86, and RMSE is 0.10 mg L^{-1}. In general, the inversion models are reliable and can be used for further research. The constructed joint inversion model and its accuracy are shown in Table 5.

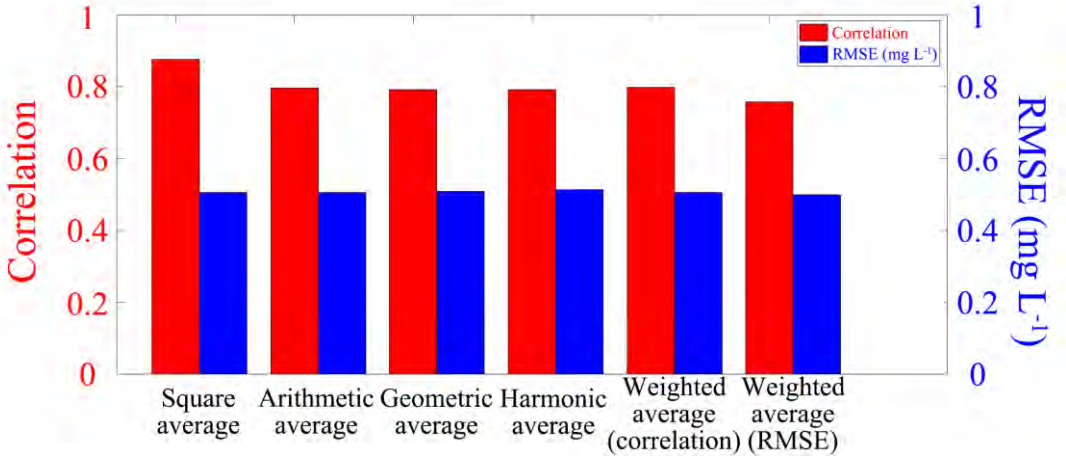

(**a**) Joint inversion models of TN

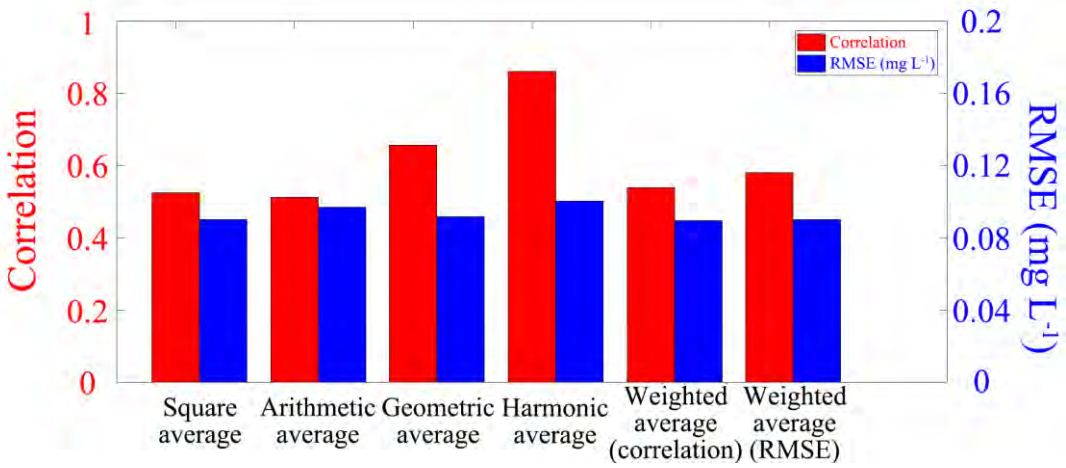

(**b**) Joint inversion models of TP

Figure 4. (**a**) The correlation and RMSE of various joint inversion models of TN. (**b**) The correlation and RMSE of various joint inversion models of TP.

Table 5. Multi-source satellite joint inversion models and evaluation indexes.

Water Quality Parameters	Joint Inversion Models	R^2	RMSE (mg L^{-1})
TN	$y = \sqrt{\frac{L^2(X_1)+S^2(X_2)}{2}}$	0.81	0.51
TP	$y = \frac{2}{\frac{1}{L(X_3)}+\frac{1}{S(X_4)}}$	0.86	0.10

where $L(X_1)$ is the optimal model of Landsat-8 for TN, $S(X_2)$ is the optimal model of Sentinel-2A about TN, $L(X_3)$ is the optimal model of Landsat-8 for TP and $S(X_4)$ is the optimal model of Sentinel-2A for TP.

The values obtained from the joint inversion model were compared with the measured values. It can be seen that the evaluation indexes of correlation and RMSE are significantly improved from the joint inversion results when compared with the single-satellite inversion results, which can better complete the task of water quality inversion. All comparison results are shown in Figure 5. The line in Figure 5 represents the measured value, and red points represent the estimated value.

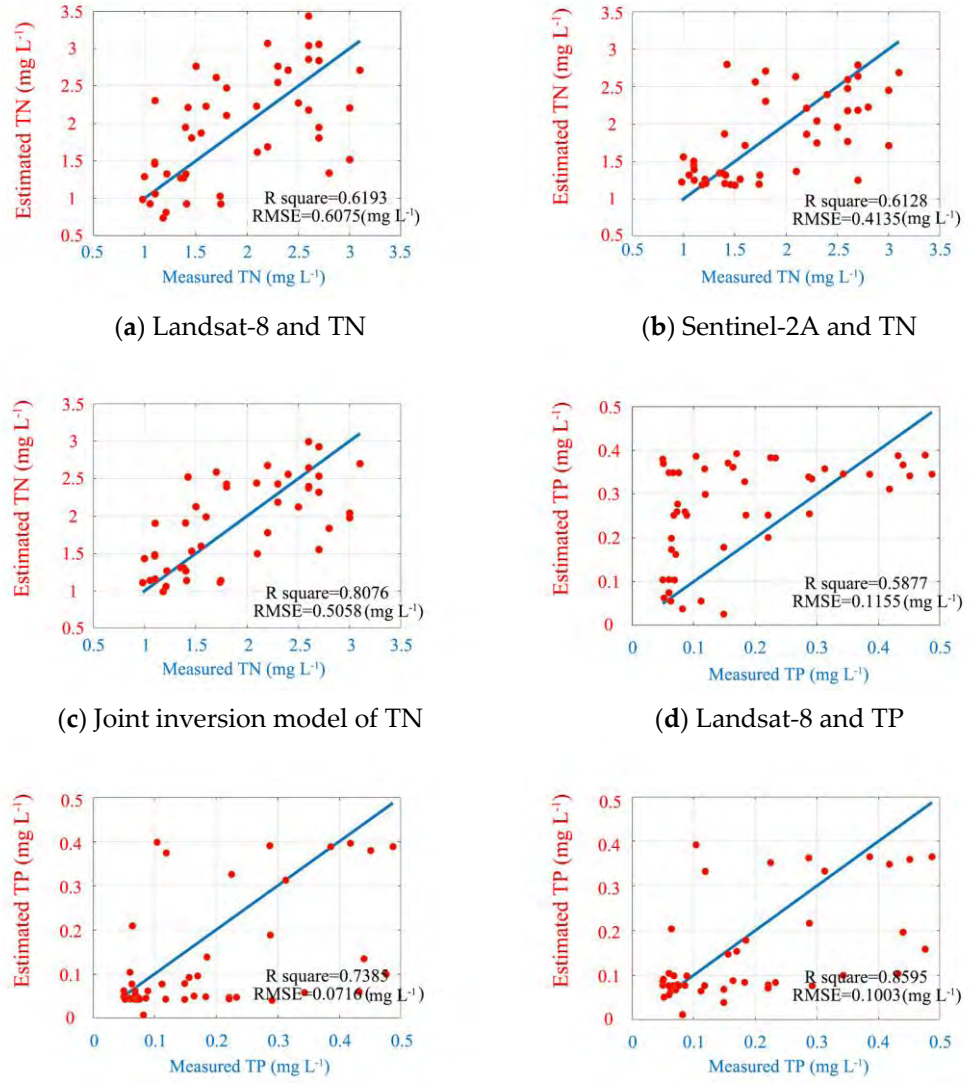

(**a**) Landsat-8 and TN (**b**) Sentinel-2A and TN

(**c**) Joint inversion model of TN (**d**) Landsat-8 and TP

(**e**) Sentinel-2A and TP (**f**) Joint inversion model of TP

Figure 5. (**a**–**c**) Comparison between measured TN and estimated TN from Landsat-8 and Sentinel-2A as well as the joint inversion model, and (**d**–**f**) Comparison between measured TP and estimated TP from Landsat-8 and Sentinel-2A as well as the joint inversion model.

3.2.2. Accuracy Analysis

The validation group data were substituted into the joint inversion models for validation, and the RMSE was used as the evaluation index for evaluation. The results are as follows: For the joint inversion model of TN, the RMSE of the validation group is 0.57 mg L^{-1}. For the joint inversion model of TP, the RMSE of the validation group is 0.1 mg L^{-1}. All results are shown in Figure 6 and Table 6.

It can be seen that the joint inversion model has a significant improvement in correlation when compared with single-satellite inversion models. In addition, although the RMSE of the inversion model obtained using the square average method and the harmonic average method is between the two single-satellite inversion models, it can better eliminate the problem that the RMSE is too large or too small due to obvious outliers while generally not affecting the model accuracy, so as to evaluate the model accuracy more objectively.

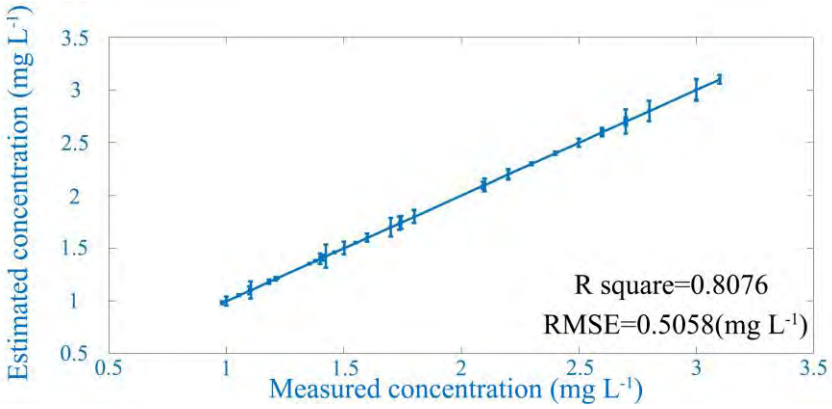

(**a**) Joint inversion model of TN

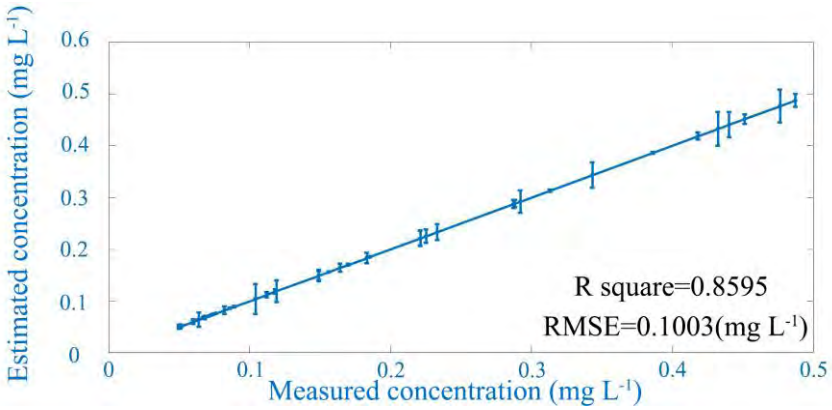

(**b**) Joint inversion models of TP

Figure 6. (**a**) Comparison between the measured concentration and estimated concentration from the joint inversion model for TN. (**b**) Comparison between the measured concentration and estimated concentration from the joint inversion model for TP.

Table 6. Accuracy analysis of joint inversion models.

Joint Inversion Models	Validation Group's RMSE (mg L^{-1})
The joint inversion model of TN	0.57
The joint inversion model of TP	0.10

3.3. Spatial-Temporal Variations of Water Quality Parameters

3.3.1. Monthly and Annual Variations

According to the results obtained above, the joint inversion models were selected with higher inversion accuracy and more stable numerical results for the inversion of TN and TP. Then, the joint inversion model was substituted into Google Earth Engine for the calculation, and a map of the changes in water quality in the main stream of the Yangtze River from 2019 to 2021 was obtained. Due to limited space, this paper only selects the changes of TN and TP in the main stream of the Yangtze River in certain months from 2019 to 2021, with a better display as shown in Figures 7 and 8.

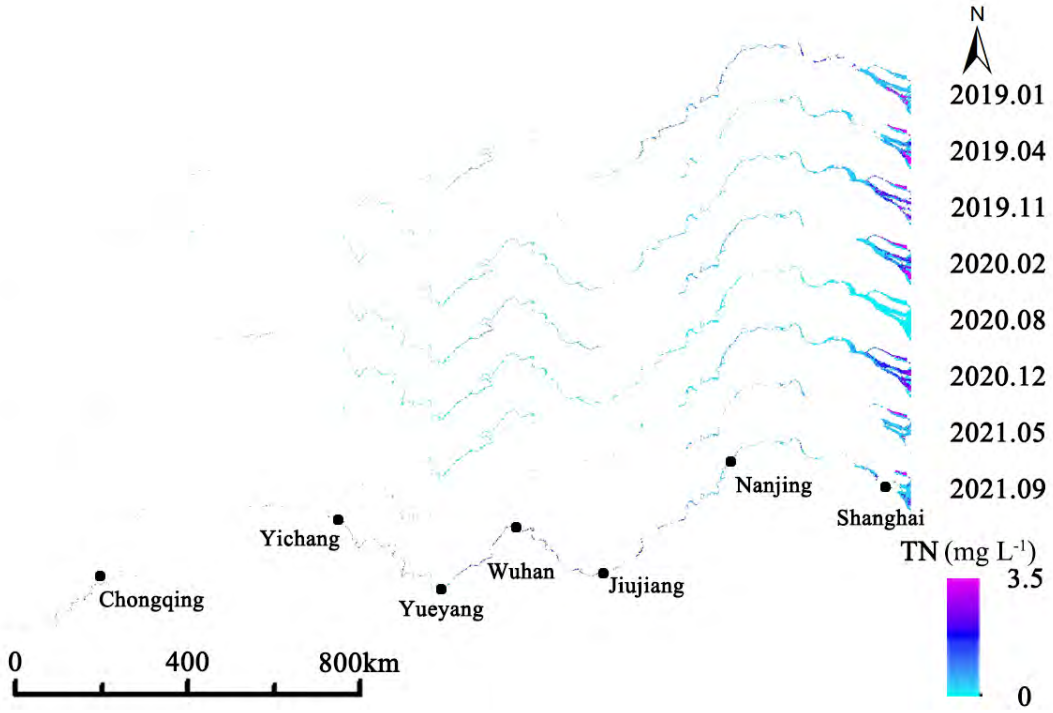

(**a**) TN

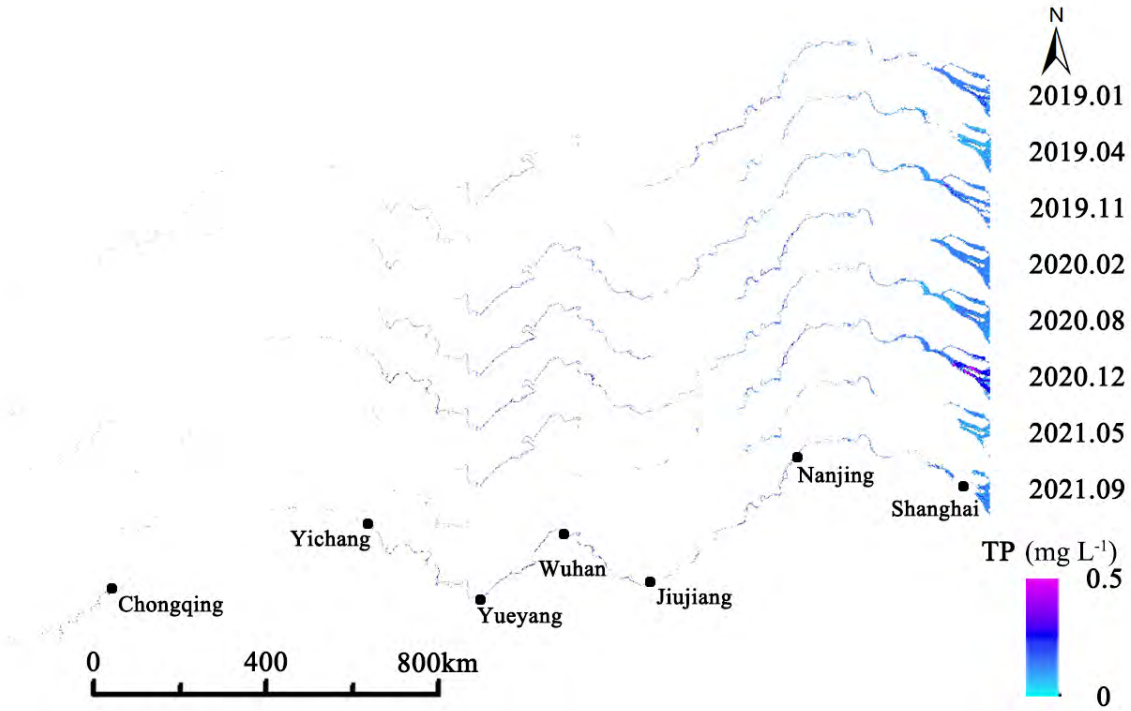

(**b**) TP

Figure 7. (**a**) Variation of TN in the main stream of the Yangtze River in some months from 2019 to 2021. (**b**) Variation of TP in the main stream of the Yangtze River in some months from 2019 to 2021.

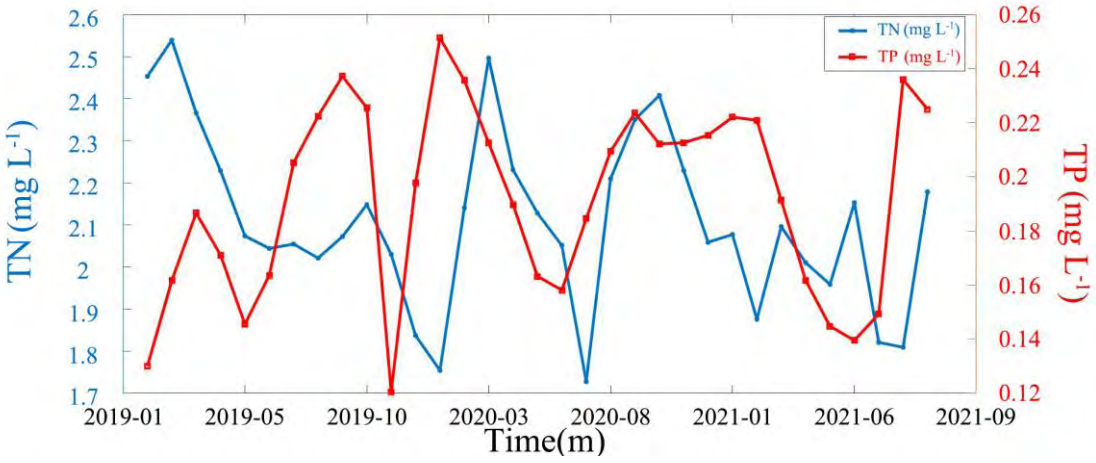

Figure 8. Monthly variation of TN and TP in the main stream of the Yangtze River from 2019 to 2021.

3.3.2. Spatial Variations

The main stream of the Yangtze River is divided into upper, middle and lower reaches. The upper reaches range from the source of the Yangtze River to Yichang, Hubei Province; the middle reaches range from Yichang, Hubei Province to Jiujiang, Jiangxi Province; and the lower reaches range from Jiujiang, Jiangxi Province to the estuary of Shanghai. Based on the obtained joint inversion models and calculation results, the changes of TN and TP in the upper, middle and lower reaches of the main stream of the Yangtze River from 2019 to 2021 are studied and shown in Figure 9.

3.3.3. Spatial-Temporal Variations of Water Quality

From 2019 to 2021, the changing trends of TN and TP in the upper, middle and lower reaches of the main stream of the Yangtze River are similar to that in the main stream of the Yangtze River overall, particularly in the lower reaches. When the water quality of the main stream of the Yangtze River changes, it is often the upstream and middle first, and then the downstream.

The water quality in the main stream of the Yangtze River has an annual variation. The water quality is poor in spring and autumn and good in summer and winter. During the years from 2019 to 2021, the annual average of TN in the main stream of the Yangtze River was 2.2 mg/L, 2.1 mg L^{-1} and 2.0 mg L^{-1}, respectively, and the annual average of TP was 0.18 mg L^{-1}, 0.21 mg L^{-1} and 0.19 mg L^{-1}, respectively, showing a declining trend year by year. The TN and TP in the upper, middle and lower reaches also showed a similar trend.

According to the evaluation standard specified in GB3838-2002, the water quality of the main stream of the Yangtze River from 2019 to 2021 was evaluated. It can be seen that the main stream of the Yangtze River is dominated by Class III water, while Class IV and V water are less common and the trend is decreasing over the time. The water quality of the main stream of the Yangtze River is converting to Class III and higher quality water. This conclusion is similar to the water quality of the main stream of the Yangtze River in the National Monthly Report of Surface Water Quality from the official website of the Ministry of Ecology and Environment of the People's Republic of China (available at https://www.mee.gov.cn/hjzl/shj/dbsszyb, accessed on 1 April 2022) in recent years.

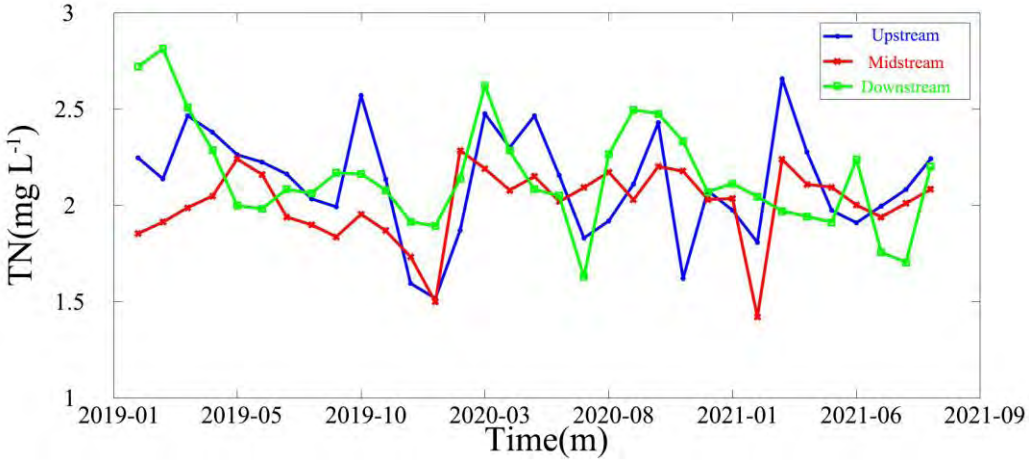

(**a**) TN

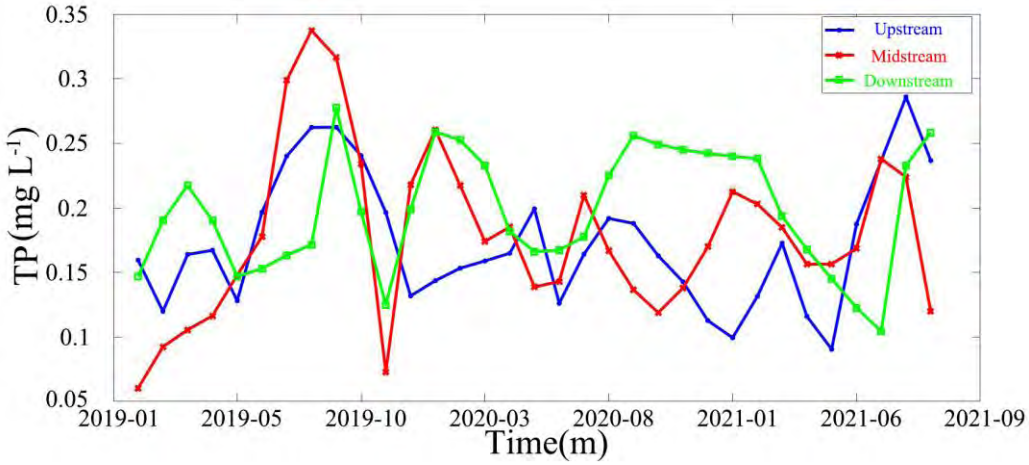

(**b**) TP

Figure 9. (**a**) Monthly variation of TN in the upstream, midstream and downstream of the Yangtze River from 2019 to 2021. (**b**) Monthly variation of TP in the upstream, midstream and downstream of the Yangtze River from 2019 to 2021.

4. Factors and Discussion

According to this research, it is found that due to the different locations of key monitoring sections on the main stream of the Yangtze River, different natural environments and local policies, the correlation between water quality and natural and human factors is also different. Considering the quality of remote sensing images in recent years, the monthly data of the hydrological monitoring station in Jiujiang, Jiangxi Province from 2019 to 2021 was selected to analyze the correlation between local water quality and hydrological, meteorological, cultural and other factors.

4.1. Hydrological and Meteorological Factors

Here three factors for water level, temperature and flow were selected to analyze the *p* value (Pearson correlation) between local water quality and hydrological and meteorological factors in Jiujiang (available at cj.msa.gov.cn and www.weather.com.cn). According to the calculations, the *p* value between the TN in the main stream of the Yangtze River in Jiujiang and the local water level is −0.76, the *p* value for the local average temperature is

−0.64, and the *p* value for the local flow is −0.69. The *p* value between the TP in the main stream of the Yangtze River in Jiujiang and the local water level is −0.64, the *p* value for the local average temperature is −0.46, and the correlation with the local flow is −0.60. The variation trends of TN and TP with water level, temperature and flow are shown in Figures 10–12 and Table 7.

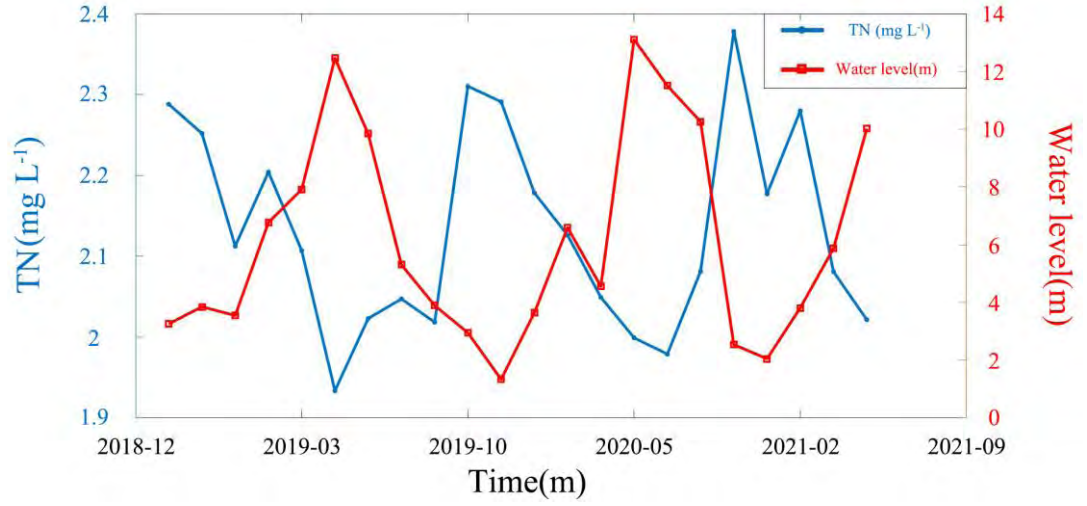

(**a**) TN and water level

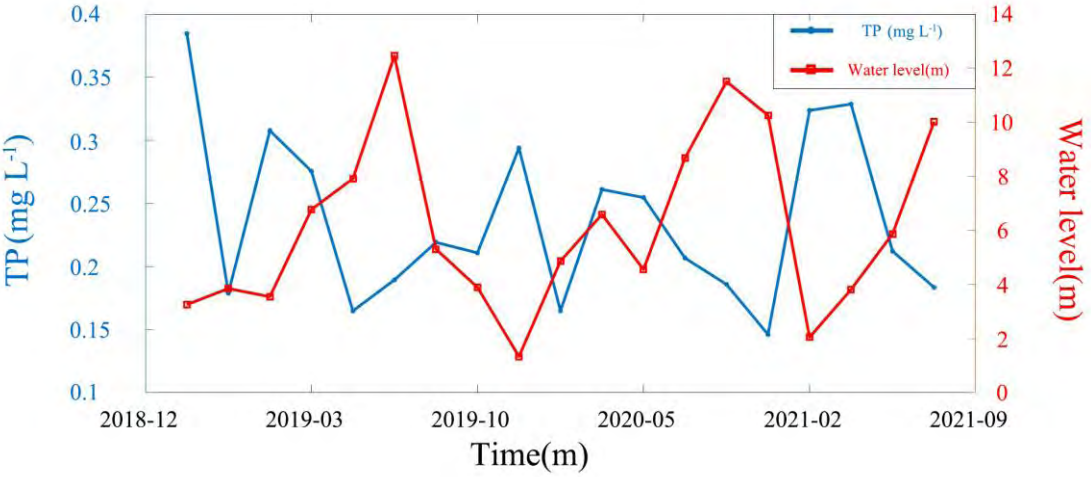

(**b**) TP and water level

Figure 10. (**a**) Monthly variation trend of TN and water level in Jiujiang from 2019 to 2021. (**b**) Monthly variation trend of TP and water level in Jiujiang from 2019 to 2021.

On the whole, TN and TP in the main stream of the Yangtze River in Jiujiang are negatively correlated with the local water level, temperature and flow. The *p* value associated with water level is higher than that of flow, and the *p* value associated with temperature is higher than that of flow.

The *p* value between TN and water level, temperature and flow data are all higher than that between TP and water level, temperature and flow data. It can be proved that the indirect evaluation or inversion of the changing trend of TN in a water body based on these hydrological and meteorological factors is more reliable. TN and TP in the main stream of the Yangtze River in Jiujiang in the same month in different years show a decreasing trend year by year, and most of the time, the local main stream of the Yangtze River belongs

to Class II water specified in GB3838-2002 issued by China. The results of this work are similar to those published by the people's Government of Jiujiang in recent years.

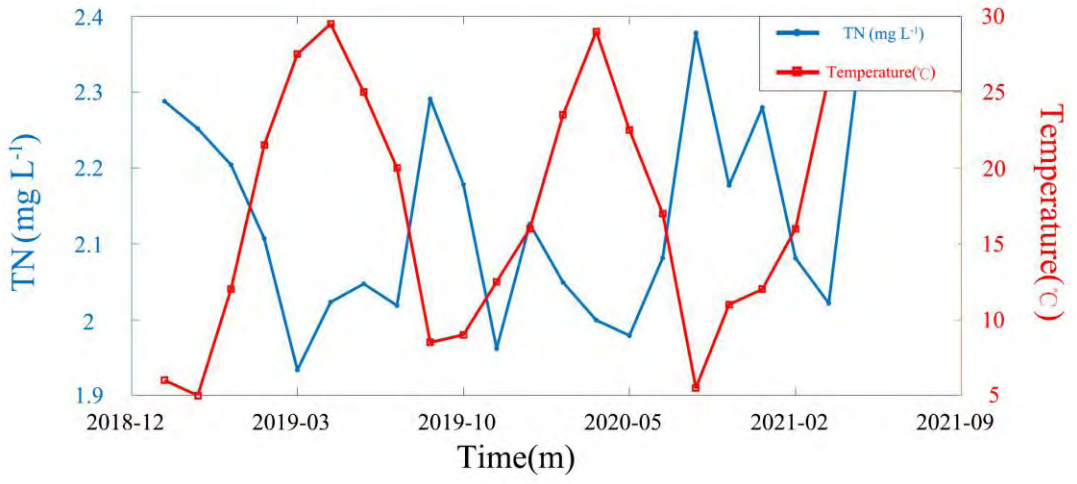

(**a**) TN and temperature

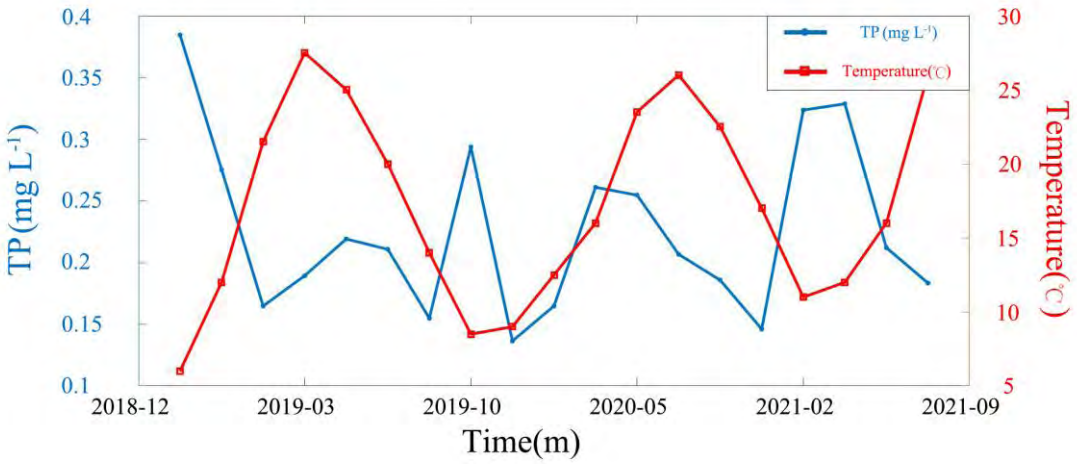

(**b**) TP and temperature

Figure 11. (**a**) Monthly variation trend of TN and temperature in Jiujiang from 2019 to 2021. (**b**) Monthly variation trend of TP and temperature in Jiujiang from 2019 to 2021.

It can be seen from the images that there are special points. TN and TP in the main stream of the Yangtze River in Jiujiang have a positive correlation with the water level, temperature and flow, most of which can be attributed to soil and water loss. In recent years, the annual announcement on Supervision and Inspection of Water and Soil Conservation of Ministry Batch Production and Construction Projects in the Yangtze River Basin and the annual announcement on Water and Soil Conservation in the Yangtze River basin (available at www.cjw.gov.cn/zwzc/gsgg, accessed on 1 June 2022) show that in 2020 alone, the area of water and soil loss in the Yangtze River Basin reached more than 330,000 square kilometers, mainly located in the upper reaches of the Yangtze River. At the same time, there is a large number of reservoirs, railways and other construction projects in the upper reaches of the Yangtze River, which is more or less unfavorable to water and soil conservation. The problems of insufficient water and soil conservation measures and non-compliance of some enterprises in the upper reaches of the Yangtze River need to be paid attention to. Water and soil loss in the upstream not only reduce the water quality in

the upstream region, but also, the pollutants in the water will flow into the middle and downstream, resulting in more serious water quality problems.

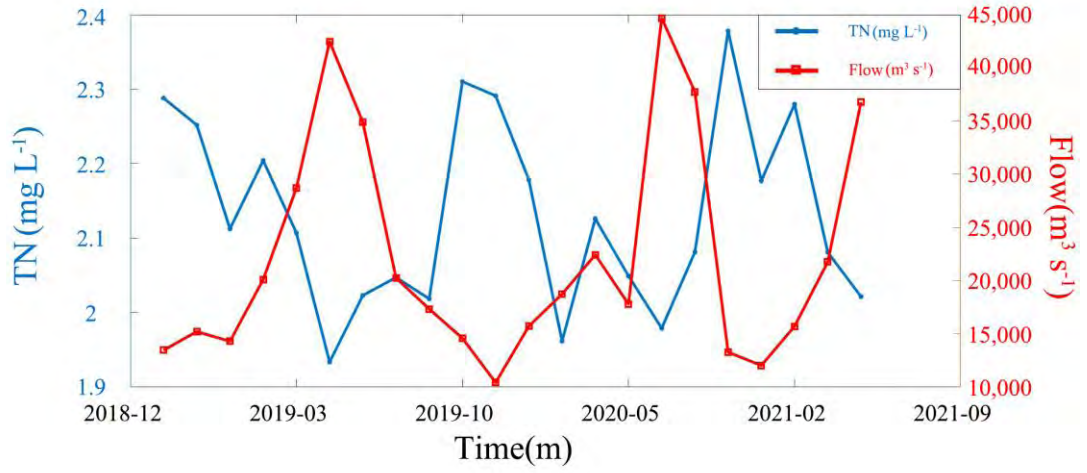

(**a**) TN and flow

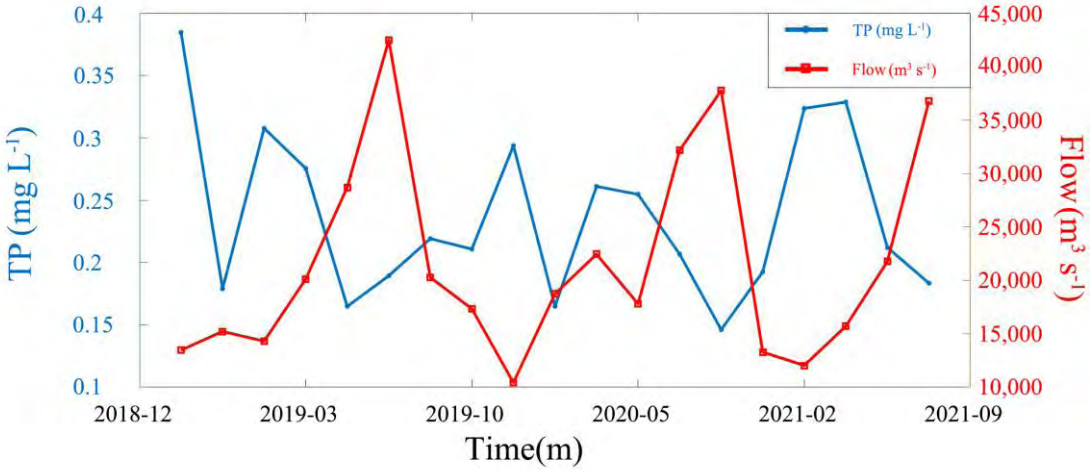

(**b**) TP and flow

Figure 12. (**a**) Monthly variation trend of TN and flow in Jiujiang from 2019 to 2021. (**b**) Monthly variation trend of TP and flow in Jiujiang from 2019 to 2021.

Table 7. *p* value between water quality parameters and hydrological and meteorological data.

Water Quality Parameters	*p* Value with Water Level	*p* Value with Temperature	*p* Value with Flow
TN	−0.76	−0.64	−0.69
TP	−0.649	−0.46	−0.60

4.2. Human Factors

According to the data in the Report on the Work of Jiujiang Municipal People's Government (available at https://www.jiujiang.gov.cn/xxgk/xzwgk/jggk/gzbg/jjszfgzgb, accessed on 1 June 2022), from 2018 to 2021, the urbanization rate of Jiujiang increased year by year at a rate of 1.5%, 1.5% and 7.7%, respectively, and the cargo throughput was also increasing steadily. These factors contribute to poor water quality, while the water quality still maintained the trend of improvement. This shows that the treatment measures taken by the municipal government—such as the construction of sewage treatment plants, the

reduction of wharfs, the repair of polluted farmland and the banning of small chemical enterprises—are effective. It can be proved that these methods are effective for water quality control and are worthy of reference in nearby areas.

The report also points out that in the past three years, Jiujiang has added more than 66.67 square kilometers of shrimp and crab breeding industry. In aquaculture, autumn belongs to the fattening period. A large amount of feed excreta will cause water eutrophication, and TN and TP in the water will rise significantly. However, from the estimated data of TN and TP in recent years, it can be seen that in autumn, TN and TP in the main stream of the Yangtze River in Jiujiang increased only slightly, which has been greatly improved when compared with previous years. This shows that the green aquaculture industry model works well and can be extended to neighboring aquaculture cities such as Suzhou and Nantong.

5. Conclusions

Based on Landsat-8 and Sentinel-2A remote sensing image data, inversion models for TN and TP in the Yangtze River were obtained from single or combining multi-source remote sensing data. The inversion accuracy is high and the results are relatively reliable from combined multi-source satellite data. Additionally, the temporal and seasonal changes in the water quality and the spatial changes in the upper, middle and lower reaches of the Yangtze River were analyzed. Most main stream of the Yangtze River is Class III with a trend of improvement year by year. The water quality in the upstream and downstream is relatively poorer, and the water quality in the middle reaches is better. TN and TP are usually higher in spring and autumn, and lower in summer and winter. Finally, the influence of hydrological and meteorological factors on the water quality in the main stream of the Yangtze River was analyzed. For example, the water level, temperature and flow data are negatively correlated with TN and TP in Jiujiang. The p value between water level and TN and TP is high, and the p value between TN and hydrometeorological factors is higher than that between TP and hydrometeorological factors. Future study will be further conducted to explore the correlation between water quality, environment, meteorology and human activities, and complete more accurate water quality monitoring and short-term prediction.

Author Contributions: Conceptualization, S.J., J.Z. and Y.Z.; methodology, J.Z. and Y.Z.; software, J.Z.; validation, S.J., J.Z. and Y.Z.; formal analysis, J.Z.; investigation, S.J. and J.Z.; data curation, J.Z. and Y.Z.; writing—original draft preparation, S.J. and J.Z.; writing—review and editing, S.J.; visualization, S.J.; supervision, S.J.; project administration, S.J.; funding acquisition, S.J. All authors have read and agreed to the published version of the manuscript.

Funding: This work was supported by the Strategic Priority Research Program Project of the Chinese Academy of Sciences (Grant No. XDA23040100) and Jiangsu Natural Resources Development Special Project (Grant No. JSZRHYKJ202002).

Data Availability Statement: The data presented in this study are available from the corresponding website.

Acknowledgments: The authors would like to acknowledge the data provided by the Changjiang Water Resources Commission of the Ministry of Water Resources.

Conflicts of Interest: The authors declare no conflict of interest.

References

1. Li, S.; Cheng, C.; Wang, X.; Li, Z. Analyzing regional economic disparities based on ESDA in Yangtze River Delta, China. In Proceedings of the 2015 IEEE International Geoscience and Remote Sensing Symposium (IGARSS), Milan, Italy, 26–31 July 2015; pp. 4530–4533.
2. Xu, J.; Liu, R.; Ni, M.; Zhang, J.; Ji, Q.; Xiao, Z. Seasonal variations of water quality response to land use metrics at multi-spatial scales in the Yangtze River basin. *Environ. Sci. Pollut. Res.* **2021**, *28*, 37172–37181. [CrossRef] [PubMed]

3. Yang, Z.; Wang, Y.; Shen, Z.; Niu, J.; Tang, Z. Distribution and speciation of heavy metals in sediments from the mainstream, tributaries, and lakes of the Yangtze River catchment of Wuhan, China. *J. Hazard. Mater.* **2009**, *166*, 1186–1194. [CrossRef] [PubMed]
4. Xu, X.; Tan, Y.; Chen, S.; Yang, G.; Su, W. Urban household carbon emission and contributing factors in the Yangtze River Delta, China. *PLoS ONE* **2015**, *10*, e0121604. [CrossRef] [PubMed]
5. Chen, P.; Wang, T.; Dong, M.; Kasoar, M.; Han, Y.; Xie, M.; Li, S.; Zhuang, B.; Li, M.; Huang, T. Characterization of major natural and anthropogenic source profiles for size-fractionated PM in Yangtze River Delta. *Sci. Total Environ.* **2017**, *598*, 135–145. [CrossRef]
6. Hui, J.; Yao, L. Analysis and inversion of the nutritional status of China's Poyang Lake using MODIS data. *J. Indian Soc. Remote Sens.* **2016**, *44*, 837–842. [CrossRef]
7. Lu, J.; Cai, H.; Fu, Y.; Zhang, X.; Zhang, W. A study on the impacts of landscape structures on water quality under different spatial scales in the Xiangjiang River Basin. *Water Air Soil Pollut.* **2022**, *233*, 163. [CrossRef]
8. Shang, W.; Jin, S.; He, Y.; Zhang, Y.; Li, J. Spatial–Temporal Variations of Total Nitrogen and Phosphorus in Poyang, Dongting and Taihu Lakes from Landsat-8 Data. *Water* **2021**, *13*, 1704. [CrossRef]
9. Di, Z.; Chang, M.; Guo, P. Water quality evaluation of the Yangtze River in China using machine learning techniques and data monitoring on different time scales. *Water* **2019**, *11*, 339. [CrossRef]
10. Xia, J.; Xu, G.; Guo, P.; Peng, H.; Zhang, X.; Wang, Y.; Zhang, W. Tempo-spatial analysis of water quality in the Three Gorges Reservoir, China, after its 175-m experimental impoundment. *Water Resour. Manag.* **2018**, *32*, 2937–2954. [CrossRef]
11. Duffy, G. Development and Optimisation of Colourimetric Microfluidic Sensors for Water Quality Monitoring. Ph.D. Thesis, Dublin City University, Dublin, Ireland, 2017.
12. Cheng, B.; Zhang, Y.; Xia, R.; Wang, L.; Zhang, N.; Zhang, X. Spatiotemporal analysis and prediction of water quality in the Han River by an integrated nonparametric diagnosis approach. *J. Clean. Prod.* **2021**, *328*, 129583. [CrossRef]
13. Gholizadeh, M.H.; Melesse, A.M.; Reddi, L. A comprehensive review on water quality parameters estimation using remote sensing techniques. *Sensors* **2016**, *16*, 1298. [CrossRef] [PubMed]
14. Guo, Q.; Wu, H.; Jin, H.; Yang, G.; Wu, X. Remote Sensing Inversion of Suspended Matter Concentration Using a Neural Network Model Optimized by the Partial Least Squares and Particle Swarm Optimization Algorithms. *Sustainability* **2022**, *14*, 2221. [CrossRef]
15. He, J.q.; Liu, N.; Han, M.l.; Chen, Y. Research on Danjiang Water Quality Prediction Based on Improved Artificial Bee Colony Algorithm and Optimized BP Neural Network. *Sci. Program.* **2021**, *2021*, 3688300. [CrossRef]
16. He, Y.; Gong, Z.; Zheng, Y.; Zhang, Y. Inland Reservoir Water Quality Inversion and Eutrophication Evaluation Using BP Neural Network and Remote Sensing Imagery: A Case Study of Dashahe Reservoir. *Water* **2021**, *13*, 2844. [CrossRef]
17. Bi, Y.-L.; Wang, H.-C.; Xia, B.; Jiang, C.-C.; Wu, W.-Y.; Li, Z.-L.; Li, S.-M.; Su, H.; Bai, Z.-H.; Xu, S.-J. Pollution Characterization and Comprehensive Water Quality Assessment of Rain-source River: A Case Study of the Longgang River in Shenzhen. *Huan Jing Ke Xue = Huanjing Kexue* **2022**, *43*, 782–794.
18. Isenstein, E.M.; Park, M.-H. Assessment of nutrient distributions in Lake Champlain using satellite remote sensing. *J. Environ. Sci.* **2014**, *26*, 1831–1836. [CrossRef]
19. Singh, K.; Jha, R. Analysing the Changes in Water Quality of River Ganga Passing Through Urban Cities with Remote Sensing and GIS Support. Asian Journal of Water. *Environ. Pollut.* **2022**, *19*, 47–58.
20. He, Y.; Jin, S.; Shang, W. Water quality variability and related factors along the Yangtze River using Landsat-8. *Remote Sens.* **2021**, *13*, 2241. [CrossRef]
21. Du, C.-g.; Li, Y.-M.; Wang, Q.; Zhu, L.; Lü, H. Inversion model and daily variation of total phosphorus concentrations in Taihu lake based on GOCI data. *Huan Jing Ke Xue = Huanjing Kexue* **2016**, *37*, 862–872.
22. Masoud, A.A. On the Retrieval of the Water Quality Parameters from Sentinel-3/2 and Landsat-8 OLI in the Nile Delta's Coastal and Inland Waters. *Water* **2022**, *14*, 593. [CrossRef]
23. Sunardi, S.; Nursamsi, I.; Dede, M.; Paramitha, A.; Arief, M.C.W.; Ariyani, M.; Santoso, P. Assessing the Influence of Land-Use Changes on Water Quality Using Remote Sensing and GIS: A Study in Cirata Reservoir, Indonesia. *Sci. Technol. Indones.* **2022**, *7*, 106–114. [CrossRef]
24. Xiang, R.; Wang, L.; Li, H.; Tian, Z.; Zheng, B. Temporal and spatial variation in water quality in the Three Gorges Reservoir from 1998 to 2018. *Sci. Total Environ.* **2021**, *768*, 144866. [CrossRef] [PubMed]
25. Niroumand-Jadidi, M.; Bovolo, F.; Bruzzone, L. Novel spectra-derived features for empirical retrieval of water quality parameters: Demonstrations for OLI, MSI, and OLCI Sensors. *IEEE Trans. Geosci. Remote Sens.* **2019**, *57*, 10285–10300. [CrossRef]
26. Bovolo, F.; Marchesi, S.; Bruzzone, L. A framework for automatic and unsupervised detection of multiple changes in multitemporal images. *IEEE Trans. Geosci. Remote Sens.* **2011**, *50*, 2196–2212. [CrossRef]
27. Caballero, I.; Steinmetz, F.; Navarro, G. Evaluation of the first year of operational Sentinel-2A data for retrieval of suspended solids in medium-to high-turbidity waters. *Remote Sens.* **2018**, *10*, 982. [CrossRef]
28. Toming, K.; Kutser, T.; Laas, A.; Sepp, M.; Paavel, B.; Nõges, T. First experiences in mapping lake water quality parameters with Sentinel-2 MSI imagery. *Remote Sens.* **2016**, *8*, 640. [CrossRef]
29. Feng, L.; Hu, C.; Han, X.; Chen, X.; Qi, L. Long-term distribution patterns of chlorophyll-a concentration in China's largest freshwater lake: MERIS full-resolution observations with a practical approach. *Remote Sens.* **2014**, *7*, 275–299. [CrossRef]

30. Markogianni, V.; Kalivas, D.; Petropoulos, G.P.; Dimitriou, E. An appraisal of the potential of Landsat 8 in estimating chlorophyll-a, ammonium concentrations and other water quality indicators. *Remote Sens.* **2018**, *10*, 1018. [CrossRef]
31. Han, L. Estimating chlorophyll-a concentration using first-derivative spectra in coastal water. *Int. J. Remote Sens.* **2005**, *26*, 5235–5244. [CrossRef]
32. Niroumand-Jadidi, M.; Pahlevan, N.; Vitti, A. Mapping substrate types and compositions in shallow streams. *Remote Sens.* **2019**, *11*, 262. [CrossRef]
33. Niroumand-Jadidi, M.; Vitti, A.; Lyzenga, D.R. Multiple Optimal Depth Predictors Analysis (MODPA) for river bathymetry: Findings from spectroradiometry, simulations, and satellite imagery. *Remote Sens. Environ.* **2018**, *218*, 132–147. [CrossRef]
34. Carvalho Júnior, O.A.; Guimarães, R.F.; Gillespie, A.R.; Silva, N.C.; Gomes, R.A. A new approach to change vector analysis using distance and similarity measures. *Remote Sens.* **2011**, *3*, 2473–2493. [CrossRef]